Photofragmentation of $OClO(\tilde{A}^2A_2\ \nu_1\nu_2\nu_3) \rightarrow Cl(^2P_J) + O_2$

R. F. Delmdahl, S. Ullrich, and K.-H. Gericke*

Institut für Physikalische und Theoretische Chemie, Technische Universität Braunschweig, Hans-Sommer-Strasse 10, D-38106 Braunschweig, Germany

Received: July 1, 1997; In Final Form: June 26, 1998

The photodissociation dynamics of $OClO(^2A_2\ \nu_1\nu_2\nu_3) \rightarrow Cl(^2P_J) + O_2$ is investigated in the wavelength region between 360 and 450 nm. Observation of nascent chlorine atom fragments produced in their electronic ground state is performed by means of three-photon excitation with subsequent recording of the vacuum ultraviolet laser-induced fluorescence. Mode-specific branching ratios between the dominant $ClO(X^2\Pi_\Omega) + O(^3P_J)$ and the minor $Cl(^2P_J) + O_2$ channel are obtained. The observed quantum yield for Cl production is determined to be below 3.6% at photolysis wavelengths between 365 and 450 nm depending on the respective vibrational level of $OClO(^2A_2\nu_1\nu_2\nu_3)$. At dissociation wavelengths below 365 nm, a sharp rise in the chlorine formation is observed resulting from a secondary photolysis step where vibrationally excited $ClO(X^2\Pi_\Omega, v \geq 4)$ radicals are dissociated.

I. Introduction

The photoinduced release of atomic halogen such as chlorine and bromine from chemical species in the stratosphere plays a crucial role in the polar ozone depletion. The reaction of chlorine and bromine radicals with ozone leads in the first step to the formation of halogen monoxides, ClO and BrO, respectively, which in turn, depending on the prevailing conditions, can readily react with each other. The reaction of BrO with ClO is known to proceed via the following three reaction pathways:[1,2]

$$ClO + BrO \rightarrow ClOO + Br \quad (1)$$

$$\rightarrow OClO + Br \quad (2)$$

$$\rightarrow BrCl + O_2 \quad (3)$$

Reactions 1 and 3 are well-established to account for a significant loss of stratospheric ozone.[3] Actually, this is not yet the case for OClO produced in pathway 2. Contrary to the kinetically unstable asymmetric ClOO, which decays instantaneously into Cl and O_2,[4,5] the symmetric OClO molecule formed in reaction 2 is photolyzed in the ultraviolet region with participation of two fragmentation channels:

$$OClO + h\nu \rightarrow ClO + O \quad (4)$$

$$\rightarrow Cl + O_2 \quad (5)$$

Although large column abundances of OClO are present in the chemically perturbed regions of the north and south polar vortex,[6−8] the possible contribution of this stratospheric trace gas to the observed overall ozone loss is not well-understood by now. In numerous laboratory studies of the OClO near-UV photochemistry in the gas phase, it was confirmed that at all wavelengths the dominating photoproducts are ClO + O (4) with only minor contribution of Cl + O_2 (5).[9−13] Since the O atom generated in this dissociation channel can react with O_2 to reform O_3, hence resulting in a net null cycle of ozone destruction, the influence of this OClO → ClO + O decay channel on the ozone layer was previously assumed to be negligible.[13,14−17] However, it has to be noted at this point that recent experiments observed the ClO fragments formed in this process containing extremely high amounts of internal energy.[18−20] As a consequence, new reaction channels which may also play a role in the chemistry of the upper atmosphere and which have hitherto been neglected taking into account only moderate internal excitation energies of the ClO radicals are thermodynamically accessible for $ClO(v \gg 0)$.

Apart from this fact, the present study is focused on the chlorine channel of the OClO fragmentation. The two aims pursued in our work are first to demonstrate that three-photon laser-induced fluorescence followed by subsequent monitoring of the total vacuum ultraviolet fluorescence is well-suitable for "soft" detection of the nascent Cl atoms without initiating secondary photolysis processes due to high-energy photons and second to use this technique to investigate the mode-selective decay of OClO into Cl atoms. A reasonable assessment of the ozone depletion potential emanating from the chlorine channel requires the accurate knowledge of the overall branching ratio between the two photolysis channels of OClO in the gas phase. Unfortunately, at the present time the quantum yields for Cl radical production reported by different groups are still controversial. In fact, in the 360 nm wavelength region, almost corresponding to the absorption maximum of OClO, Donaldson and co-workers[21,22] reported a Cl quantum yield in the order of up to 15%, while Apkarian et al.[23] and Davis and Lee[12,13] in the same region found a Cl yield of nearly 0%. According to atmospheric model calculations, a 10% total quantum yield of the chlorine channel 5 would already account for a 3% overall Antarctic ozone depletion.[24] Considering this possible impact of stratospheric chlorine dioxide, the prevailing uncertainty with regard to the relative amount of Cl formation occurring from the photolysis of OClO is not quite satisfactory. Against this background, the work presented in this paper aims at a reexamination of the wavelength-dependent quantum yields over the entire OClO near-UV absorption band.

S1089-5639(97)02111-7 CCC: $15.00
Published on Web 08/21/1998

II. Experimental Details

The experimental setup consists of two pulsed tunable laser systems. The photolysis wavelength is provided by a dye laser (Lambda Physik FL 3002), which is pumped by a XeCl excimer laser (Lambda Physik LPX 100). A second dye laser (Radiant Dyes DL-midi) pumped by a XeCl excimer laser (Radiant Dyes RD-EXC-200) is employed for state-selective detection of the nascent fragmentation products. The photolysis laser pulse energies are between 3 and 14 mJ depending on the respective wavelength at a pulse duration of 15 ns and a laser bandwith of 0.4 cm^{-1}. At the used laser intensities and the respective absorption cross sections,[25] the photodissociation of OClO was calculated to proceed at all times in saturation. Both the photolysis and the detection laser enter the reaction chamber counterpropagating and time-delayed. Both lasers are focused by a quartz lenses. The output of the dye laser used for detection is always above 10 mJ/pulse at a pulse duration of 15 ns. The detection laser bandwidth is below 0.1 cm^{-1}. To minimize unwanted one-color photolysis conditions, it is necessary that the detection beam volume is entirely enclosed by the photolysis beam volume in the interior of the reaction cell. This is achieved by using a 300 mm quartz lens for the photolysis beam and a 250 mm quartz lens for the detection beam. To check the saturation condition for the OClO absorption, the influence of the photolysis intensity on the observed Cl signal was investigated over a broad spectral range. Changes of the Cl signal were observable only at photolysis energies below 4 mJ/pulse. Since the measurements were carried out above 10 mJ/pulse, saturation of the photolysis is assured. This experimental result is confirmed by calculations considering the laser intensities and focusing conditions. Observation of the nascent photolysis products emanating from the two dissociation channels, Cl and ClO fragments, respectively, is performed employing multiphoton laser-induced fluorescence (LIF) techniques. The detection scheme for nascent state-resolved ClO detection by two-photon LIF as well as the laser beam arrangement have been described in detail in previous reports.[18,26] To detect the Cl($3p^2P_J$) atoms formed in channel 5, the $3p^2P_J \rightarrow 4s^2P_J$ ($J = {}^1/_2, {}^3/_2$) transitions are probed by resonant absorption of three photons at an excitation wavelength near 404 nm followed by subsequent monitoring of the total vacuum ultraviolet fluorescence near 135 nm with a solar-blind photomultiplier tube (EMR 542-G-08-18) perpendicular to the laser beams. The output of the photomultiplier is fed into a boxcar averager (SRS 250) and after A/D conversion stored in a computer. All time events are controlled by a trigger device (SRS DG 535). The relatively long Cl excitation wavelength applicable in this method provides two distinct advantages. One is the spectral discrimination between the detection laser photons and the fluorescence photons. The second advantage, being of crucial importance, is the prevention of secondary photolysis processes, where the ClO radical of the major channel 4 is photodissociated into Cl and O atoms, and thus pretending an enhanced Cl/ClO branching ratio of the OClO photolysis. A time delay between photolysis and detection laser pulse of 100 ns and a total cell pressure of 100 mTorr allows the detection of nascent Cl($3p^2P_J$) photofragments.

OClO is prepared by slowly letting flow a 10% mixture of chlorine diluted in nitrogen at atmospheric pressure through a glass tube of 50 cm in length and 5 cm in diameter filled with sodium chlorite and glass beads.[27] To obtain a quantitative yield of the OClO product, the Cl_2/N_2 gas mixture is directed through water before flowing through the $NaClO_2$-containing glass column.[13] OClO should be kept below 200 mbar partial pressure and at room-temperature conditions because of its explosive character. The yellowish in situ reaction product obtained with this method is led to the reaction cell via glass and Teflon tubings.

To calibrate the Cl fluorescence signal resulting from OClO dissociation, a glass vessel containing a mixture of neat chlorine diluted in nitrogen is additionally connected to the reaction chamber via a bypass.

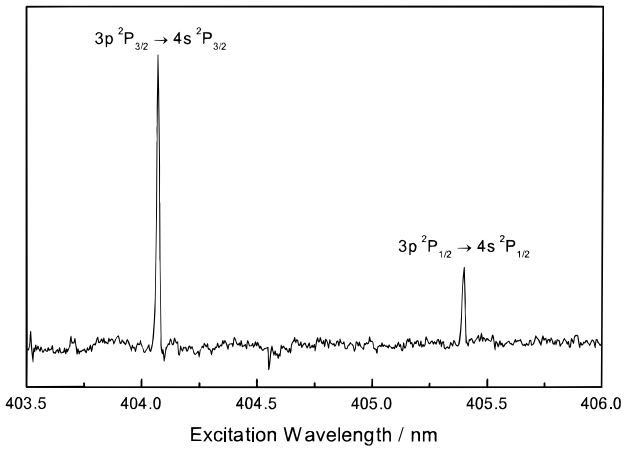

Figure 1. Three-photon LIF spectrum of Cl(^2P_J) occurring from the OClO(5, 1, 0) initial state.

TABLE 1: Three-Photon Excitation Wavelengths and Relative Transition Probabilities[28] of the Single ($3p^2P_J \rightarrow 4s^2P_J$) Transitions

($3p^2P_J \rightarrow 4s^2P_J$) transition	three-photon wavelength/nm	relative transition probability
3/2 → 1/2	400, 72	1/9
3/2 → 3/2	404, 08	5/9
1/2 → 1/2	405, 40	2/9
1/2 → 3/2	408, 94	1/9

III. Results

Figure 1 shows the (3 $h\nu$) LIF spectrum of Cl obtained from the 404 nm photolysis near the OClO($^2A_2$ 5, 1, 0) mode. This spectrum is recorded with the dissociation laser held fixed at a wavelength of 404 nm, whereas the detection laser wavelength is tuned across the $3p^2P_J \rightarrow 4s^2P_J$ spin−orbit transitions of Cl(^2P_J). In Figure 1 two of four possible peaks, the $^2P_{3/2} \rightarrow {}^2P_{3/2}$ and the $^2P_{1/2} \rightarrow {}^2P_{1/2}$ spin−orbit transition, respectively, are shown. Since the population of the Cl($3p^2P$) $J = {}^1/_2$ and $J = {}^3/_2$ spin−orbit states is not observed to depend on the initial OClO($\nu_1\nu_2\nu_3$) mode, the strong $3p^2P_{3/2} \rightarrow 4s^2P_{3/2}$ transition is always used for the mode-selective determination of the Cl atom quantum yield. The transition probabilities of the ($3p^2P_J \rightarrow 4s^2P_J$) transition of Cl, as calculated by Reinsch,[28] are represented in Table 1.

To calibrate the fluorescence signal obtained in the one-color OClO photolysis at 404 nm, a 0.1% mixture of neat chlorine diluted in nitrogen is pumped through the reaction chamber. The change of the (3 $h\nu$) LIF signal of Cl resulting from Cl_2 photodissociation at a wavelength of 404 nm as a function of the total cell pressure is seen in Figure 2. The observed linear behavior of the Cl LIF signal in the applied pressure range makes sure that the signal intensity is solely dependent on the number of Cl products and that this scheme for Cl detection is suitable for the determination of the ClO/Cl branching ratio. By this means the absolute (3 $h\nu$) LIF detection limit of chlorine atoms is found to be in the order of 10^9 cm^{-3}. The quantum

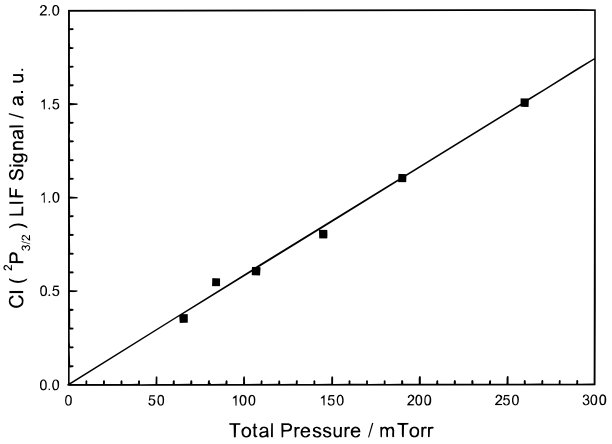

Figure 2. Pressure dependence of the Cl fluorescence signal obtained from the OClO(5, 1, 0) photolysis.

yield of Cl products can be calculated from the following expression

$$\frac{S(\mathrm{OClO})}{S(\mathrm{Cl_2})} = \frac{\Phi_{\mathrm{Cl}}(\mathrm{OClO})\cdot \mathrm{P}_J(\mathrm{OClO})\cdot[\mathrm{OClO}]}{\Phi_{\mathrm{Cl}}(\mathrm{Cl_2})\cdot \mathrm{P}_J(\mathrm{Cl_2})\cdot[\mathrm{Cl_2}]} \qquad (6)$$

where S is the observed fluorescence signal, Φ_{Cl} is the quantum yield of Cl formation (obviously Φ_{Cl} (Cl_2) equals 2), and P_J is the population of the Cl(^{2}P) spin−orbit state.

As a result, from the one-color OClO photolysis near the OClO(5, 1, 0) state the Cl yield was determined to 3.6%. On the basis of the transition probabilities given in Table 1, the Cl* fraction f_{Cl^*} = Cl*/(Cl + Cl*) was determined for the photolysis of both Cl_2 and OClO. In the case of Cl_2 a value of $f_{\mathrm{Cl}^*}(\mathrm{Cl_2}) = 0.36$ was observed, while in the photolysis of OClO a fraction of $f_{\mathrm{Cl}^*}(\mathrm{OClO}) = 0.40$ was found. The error in determining f_{Cl^*} is estimated from the signal-to-noise ratio to be $\Delta f = \pm 0.02$. A possible error in the calculated transition probabilities might result from the neglect of particular spin−orbit couplings. However, it is reasonable to assume that the obtained values (Table 1) agree within a few percent with the exact transition probabilities. Thus, the influence of these errors on the relative Cl quantum yield should be in the order of merely a few percent. The accuracy of the determination of the total quantum yield of Cl atoms in the photodissociation of OClO, however, essentially depends on the calibration procedure using Cl_2 as the reference system and only to a minor extent on the specific spin−orbit branching ratios and the transition probabilities. Since in performing the calibration measurements the experimental setup remained unchanged (only Cl_2 and OClO had to be exchanged), we expect an error of about 10% in the obtained quantum yield.

To determine the Cl quantum yields originating from various OClO(ν_1, ν_2, ν_3) states, several action spectra are recorded in the structured region of the OClO absorption spectrum. In the corresponding spectra depicted in Figure 3a−c the photolysis wavelength is varied over several neighboring OClO modes whereas the detection wavelength is held fixed on the ($3p^2P_{3/2} \rightarrow 4s^2P_{3/2}$) transition of Cl.

Although three-photon LIF is a suitable means for nascent Cl ($3p^2P_J$) detection, one problem arises from the fact that the applied probe wavelength of 404 nm corresponds essentially to the ($^2A_2$ 5, 1, 0) vibrational band of the OClO absorption spectrum. As a consequence, a fraction of the observed Cl fragments may be formed in the one-color OClO photolysis process induced by the detection laser, if not all OClO molecules

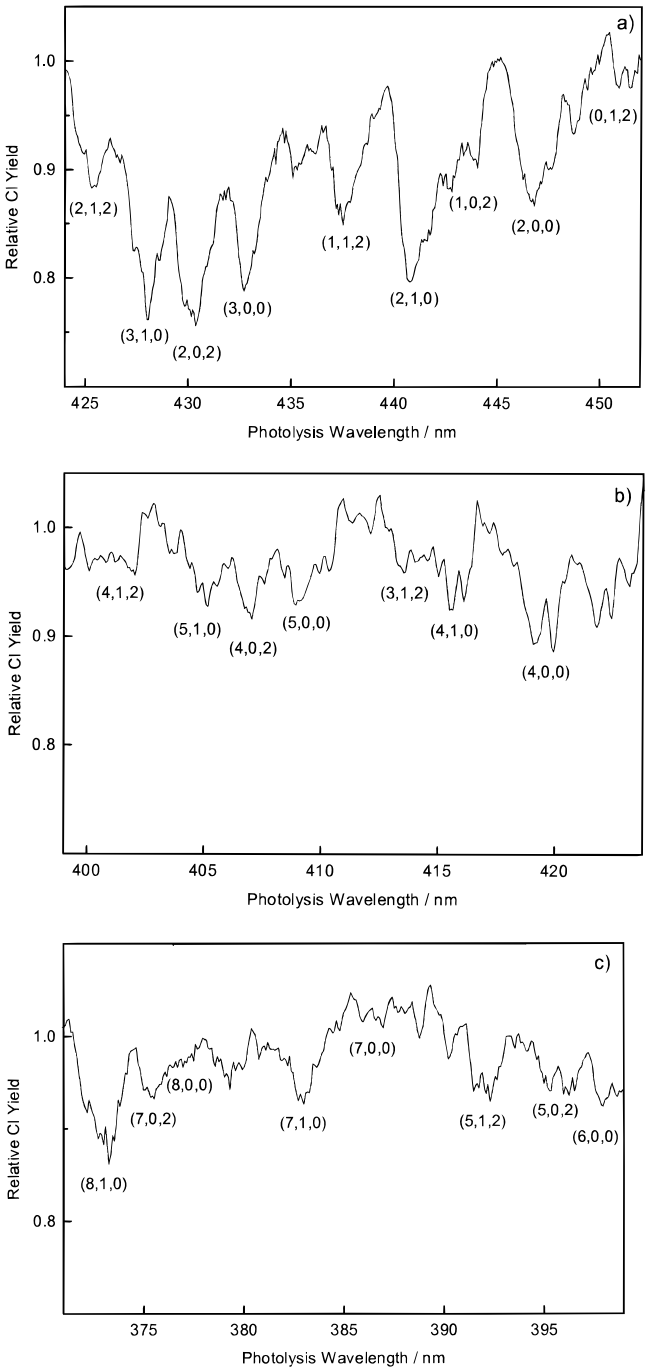

Figure 3. (a−c): Three-photon LIF action spectra of ground-state Cl ($^2P_{3/2}$) obtained from the photofragmentation of OClO(ν_1, ν_2, ν_3). The Cl yields obtained from the different OClO modes are normalized to the Cl yield of 3.6% determined from the 404 nm one-color photolysis.

are dissociated by the photolysis laser beam, which is the case when the photolysis laser is tuned between the $^2A_2$(ν_1, ν_2, ν_3) modes. For this reason, the experimentally obtained quantum yield of Cl arising from the various initial vibrational states of OClO are in the following given in relation to the Cl yield, which is determined at a wavelength of 404 nm, where the Cl formation is unambiguously resulting from a defined dissociation wavelength.

The spectra in total extending from 370 to 452 nm exhibit a clear mode dependence of the quantum yield, apparently most pronounced in the wavelength region between 425 and 450 nm (see Figure 3a), where the Cl quantum yield of different OClO-(ν_1, ν_2, ν_3) initial states exhibit the strongest decrease relative

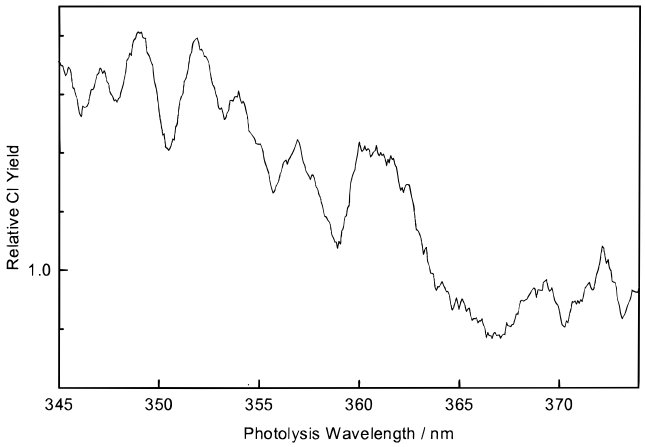

Figure 4. Three-photon Cl($^2P_{3/2}$) LIF action spectrum recorded in the wavelength region between 345 and 375 nm, exhibiting a steep increase of the Cl quantum yield near 360 nm.

to the yield obtained from the 404 nm photolysis. The observed peaks can easily be assigned to the corresponding OClO(ν_1, ν_2, ν_3) modes. At this point, it is necessary to explain the apparent OClO modal features appearing generally as minima in the action spectra. Actually, this is the result of the above-described one-color photolysis contribution of the detection laser. A decrease of the Cl quantum yield produced from a particular OClO(ν_1, ν_2, ν_3) initial state relative to the Cl yield obtained from the one-color OClO photolysis causes a downward pointing of the OClO mode in the action spectrum and vice versa. As already mentioned above, the detection wavelength is held fixed on the ($3p^2P_{3/2} \rightarrow 4s^2P_{3/2}$) transition of Cl at 404 nm (cf. Table 1). Obviously, only downward pointing modes are observed at photolysis wavelengths between 365 and 452 nm (Figure 3a−c). This observation proves that the Cl formation in this spectral region of the OClO absorption spectrum is relatively lowered with respect to the Cl yield obtained from the 404 nm OClO photolysis near the (5, 1, 0) state. In accordance with our observation, the OClO(5, 1, 0) state was experimentally found by Davis and Lee[12,13] to represent the region of maximum Cl production.

As shown in Figure 4, at photolysis wavelengths below 365 nm a sudden increase in the Cl quantum yield is observable. Moreover, in this region only a few spectral features are assignable to the OClO(ν_1, ν_2, ν_3) states such as the first broad peak corresponds to excitation of the (9, 0, 2) and (10, 1, 0) states. However, there are other peaks that have no correspondence in the OClO absorption spectrum, indicating that the Cl atoms originate from a different source. Since ClO fragments are simultaneously formed with a high quantum yield in the major channel 4, the secondary photolysis of these products might be the source of Cl atoms in the wavelength region below 365 nm. Although the ClO($A^2\Pi$, $v' \leftarrow X^2\Pi$, $v = 0$) absorption band represented in Figure 5 (taken from ref 29) only extends to around 310 nm, the absorption cross section will be sufficiently shifted to the red if ClO(v) products are generated in vibrationally excited states. Following this suggestion, the internal energy distribution of ClO(v, J) radicals generated in the 360 nm photolysis is examined using two-photon LIF. This method is described in detail in a previous paper.[18] Obviously, the resulting ClO($C^2\Sigma$, $v' = 0 \leftarrow X^2\Pi$, v) ($2h\nu$) LIF spectrum, which is shown in Figure 6, clearly proves the ClO fragments at this photolysis wavelength to be formed in ($v \leq 4$) vibrational states. Hence, photodissociation of the vibrationally hot ClO fragments accounts for the observed rapid increase of the Cl formation at photolysis wavelengths below

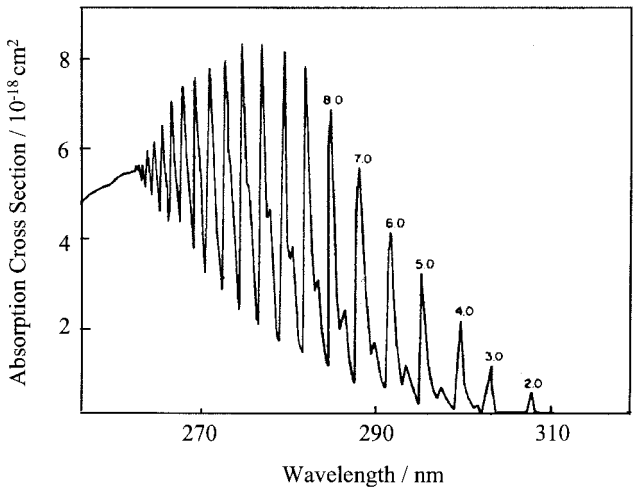

Figure 5. ($A^2\Pi$, $v' \leftarrow X^2\Pi_\Omega$, $v = 0$) absorption band of ClO (taken from ref 29).

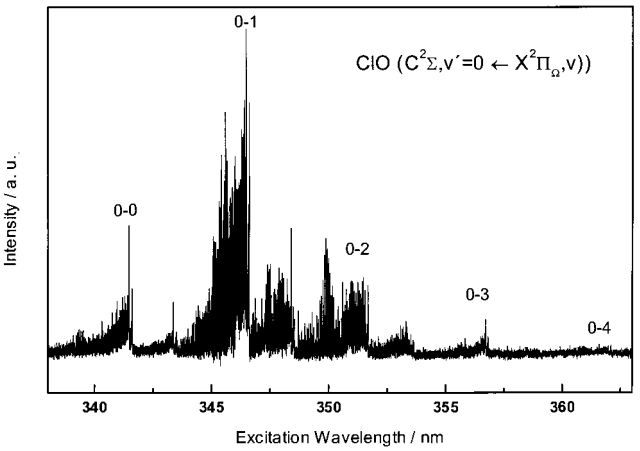

Figure 6. Two-photon ($C^2\Sigma$, $v' = 0 \leftarrow X^2\Pi_\Omega$, v) LIF spectrum of ClO radicals formed in the OClO photolysis at 360 nm.

360 nm. The mode structure of the respective action spectrum is consequently the result of both the structured OClO and the structured ClO absorption band. Although, for this reason, the quantum yield of the Cl channel cannot be determined exactly for highly excited OClO($\nu_1 > 10$) initial states in the short wavelength regime, it has to be mentioned at this point that the internal energy distribution of ClO(v, J) radicals generated from OClO($\nu_1 > 14$) indicates the increasing onset of a direct predissociation mechanism presumably favoring significantly the ClO channel.[19,20]

IV. Discussion

This work demonstrates that the ($3h\nu$) laser-induced fluorescence technique using the ($3p^2P \rightarrow 4s^2P$) system is well-suitable for the detection of chlorine atoms especially when a relatively low photon energy is needed. Another sensitive technique that is often employed for Cl detection is (2 + 1) resonance-enhanced multiphoton ionization (REMPI) using several (3p4p) two-photon transitions in the wavelength region between 230 and 245 nm.[10,11,30] Obviously, the corresponding detection wavelengths are not appropriate for the determination of the ClO/Cl branching ratio owing to strong absorbance of ClO radicals in this spectral region,[31] which in turn provides an additional source for Cl atom formation. This explains the formerly observed high Cl quantum yield when the (2 + 1) REMPI detection technique was used.

The essential part of this work is the measurement of the chlorine quantum yields obtained in the photodissociation of OClO($^2A_2$ ν_1, ν_2, ν_3). This is easily feasible in the spectral region between 365 and 452 nm applying three-photon laser-induced fluorescence detection of the formed chlorine atoms. The quantum yields are determined from action spectra using molecular chlorine for calibration purposes.

The spectral features (Figure 3a−c) exhibit Cl yields below 3.6% in the 365−450 nm region of the OClO absorption spectrum. Hence, the observed Cl quantum yields from the various OClO(ν_1, ν_2, ν_3) levels are of the same order of magnitude as those reported by Davis and Lee,[13] which used photofragment translational energy spectroscopy. Like Davis and Lee we also observed mode-specific behavior of the Cl yield as indicated by the mode structure of the action spectra (Figure 3a−c). The mode selectivity is most pronounced at very low dissociation energies between 425 and 452 nm. In the corresponding action spectrum (Figure 3a) the alteration of the Cl quantum yields is about twice as much than at all shorter photolysis wavelengths between 425 and 365 nm (Figure 3b,c). Additionally, the total quantum yield in the long wavelength region above 425 nm (>2.9 eV) is somewhat decreased with respect to higher excitation energies (cf. Figure 3a−c). At wavelengths shorter than 425 nm the mode structure is apparently weaker. A sudden increase in the Cl quantum yield is noticed near 360 nm (Figure 4), where only a few spectral features are assignable to OClO vibrational states, thus indicating a secondary source of Cl formation.

While OClO is electronically excited from the X^2B_1 ground state to the dipole-allowed A^2A_2 state, the photofragmentation process is generally influenced by two further electronically excited states, namely $^2A_1$ and $^2B_2$, which lie close in energy with the initially prepared A^2A_2 state. Interaction between these excited states is known to occur via spin−orbit coupling for the A^2A_2 and the $^2A_1$ states, whereas the $^2A_1$ and the $^2B_2$ states can interact by vibronic (ν_3) coupling. Concerning the ClO + O channel, recent calculations by Peterson and Werner[32] show that both the A^2A_2 and the $^2A_1$ states exhibit barriers of around 3.1 eV to ClO and O products near the OClO equilibrium angle, whereas the $^2B_2$ state is essentially unbound along the (ν_3) coordinate. Consequently, at excitation energies that exceed the barriers in principle all three surfaces can participate in the decay into ClO and O, which has apparently been observed in various experimental results.[12,13,15,18−20]

The formation of Cl and O_2 products, however, is expected to be strongly favored by symmetric motions, namely, the symmetric stretch (ν_1) and the bend (ν_2), which was already observed in previous investigations.[12,13] Very recently Peterson and Werner calculated C_{2v} potential energies for the X^2B_1, A^2A_2, $^2A_1$, and the $^2B_2$ state of OClO.[33] According to their theoretical results, when constrained to C_{2v} geometry the X^2B_1, A^2A_2, and $^2A_1$ states exhibit large barriers of 4.6, 4.4, and 4.8 eV, respectively. The $^2B_2$ surface in C_{2v} geometry is bound to Cl and O_2 formation as well, albeit only up to 2.86 eV. However, as depicted in Figure 7, from their calculations Peterson and Werner found a dramatic decrease of the $^2B_2$ barrier height following successive breaking of the C_{2v} symmetry. With increasing asymmetry, however, the system becomes more and more unbound with respect to ClO and O products. The experimental results of our work can essentially be explained in accordance with the above theoretical findings.

A. Distinct Mode Specifity at Excitation Energies below 2.9 eV (λ > 425 nm). At excitation wavelengths longer than 425 nm (Figure 3a), the decay of OClO in C_{2v} geometry is

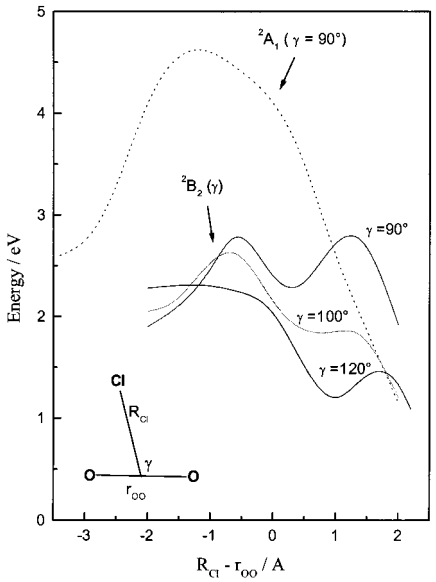

Figure 7. C_{2v} and C_s minimum energies, respectively, for the reaction of OClO to Cl + O_2 along the $^2A_1$ and $^2B_2$ states (both become $^2A'$ in C_s geometry) calculated by Peterson and Werner.[33] R_{Cl} is the distance of the Cl atom to the center of gravity of the O atoms, r_{OO} is the distance between the O atoms, and g, is the angle between R_{Cl} and r_{OO}.

energetically not possible in terms of the calculated C_{2v} barriers. As predicted by the theoretical calculations of Peterson and Werner,[32,33] at these low excitation energies the dissociation is only indirectly possible along the $^2B_2$ state under non-C_{2v} conditions (Figure 7). However, with increasing C_s symmetry, the $^2B_2$ surface becomes unbound also with respect to dissociation into ClO and O. As a result, the Cl yield should be decreased in favor to the competing ClO channel. In fact, this behavior is actually observed in the respecting wavelength region corresponding to photolysis energies up to 2.9 eV, which equals rather exactly the C_{2v} energy barrier of 2.86 eV of the $^2B_2$ surface. Furthermore, it is clearly observable from Figure 3a that the influence of the initial OClO($\nu_1\nu_2\nu_3$) mode is relatively enhanced with respect to shorter photolysis wavelengths, the respective Cl yield varying between 2.7% and 3.6%. This experimental observation appears reasonable considering the fact that C_{2v} geometries or, as in this case with energies below the C_{2v} barrier of the $^2B_2$ state, at least near C_{2v} geometries are required to avoid formation of ClO and O products along the barrierless (ν_3) coordinate of the $^2B_2$ state. Consequently, the competition between the ClO and the Cl channel, i.e., whether the near-C_{2v} energy barrier of the $^2B_2$ state leading to the Cl + O_2 products is crossed, depends in a sensitive way on the initial vibrational motion of the A^2A_2 excited OClO parent molecule. From their time-of flight spectra Davis and Lee were able to estimate the electronic state distributions of the O_2 fragments, which indicate a considerable O_2 yield resulting from the $^2A_1$ state according to orbital symmetry considerations. This observation is explained by conical intersections between the $^2A_1$ and the $^2B_2$ states (both $^2A'$ in C_s symmetry) late in the exit channel, since no mode specifity of the O_2 electronic state formation is observed. Davis and Lee as well found a distinct mode selectivity of the Cl formation together with slightly decreased Cl quantum yields in the 425−450 nm region. The differences in the mode-specific behavior of the Cl yields compared to our action spectrum (Figure 3a) are probably due to the different experimental accuracy. However, it might be mentioned that neighboring modes in the three-photon LIF action spectrum are obtained in a single experimental run, whereas each Cl quantum yield obtained by the universal

detector is the result of separately recorded time-of-flight profiles. Therefore, comparing neighboring initial OClO(ν_1, ν_2, ν_3) modes, the relative error in our experiment should be fairly low.

B. Decreased Influence of the OClO(ν_1, ν_2, ν_3) State at Energies above 2.9 eV (λ < 425 nm). At energies above the C_{2v} barrier of $^2B_2$, the formation of Cl and O_2 fragments is no longer constrained to near-C_{2v} symmetries. Thus, the Cl yield is expected to be enhanced compared to excitation energies below 2.9 eV, which is indeed observed at the corresponding photolysis wavelengths (see Figure 3b,c). Since now symmetric motions such as the symmetric stretch and the bending mode as well as slight asymmetric distortions induced by the asymmetric stretch partially favor the Cl channel, the significance of the single OClO modes is generally decreased. Correspondingly, in our experiment the dependence of the Cl yield on the respective OClO mode is not as significant at excitation wavelengths above 2.9 eV, varying only slightly around 3.3%.

C. Onset of the Secondary Fragmentation Process ClO($v \geq 4$) → Cl + O near 360 nm. Previously, the Cl quantum yield of the OClO photolysis near 360 nm was investigated,[10,11,21,22] and a relatively high Cl quantum yield of 10−15% was reported. Actually, an overall quantum yield of Cl in this order of magnitude following OClO photodissociation should already have an effect on the stratospheric ozone concentration according to recent assumptions made by Vaida and Simon.[24] However, this high quantum yield is likely due to fragmentation of ClO(v) products formed in vibrationally excited states in the major channel. The onset of this additional source for Cl production is already observable at wavelengths near 360 nm, as is seen in Figure 4. When the (2 + 1) REMPI technique for Cl detection at much shorter wavelengths around 235 nm is used, the observed Cl quantum yield should be strongly influenced by the photolysis of ClO radicals. As is obvious from our experiments (see Figure 4) the unambiguous measurement of Cl quantum yields following OClO photodissociation is generally not possible at photolysis wavelength below 365 nm owing to simultaneous ClO(v) fragmentation in this wavelength region.

V. Conclusion

In our work we have demonstrated that the detection of halogen atoms is feasible at relatively long wavelengths by employing a three-photon laser-induced fluorescence method. We have investigated the Cl quantum yields arising from OClO($^2A_2$ ν_1, ν_2, ν_3) photofragmentation at wavelengths between 360 and 450 nm. Cl (^2P_J) radicals are for the first time detected by means of three-photon LIF. The Cl quantum yields were determined to be below 3.6%, hence, at present knowledge, not affecting the atmosphere. In the 360 nm region a steep increase of the Cl yield is observed resulting from photolysis of vibrationally excited ClO. The influence of this process on the Cl concentration in the stratosphere depends on the solar flux and the relaxation rate of ClO(v).

Acknowledgment. Support of this work by the Deutsche Forschungsgemeinschaft is gratefully acknowledged. In addition, we thank Prof. E. A. Reinsch for calculating the relative transition probabilities for the three-photon excitation of Cl.

References and Notes

(1) McElroy, M. B.; Salawitch, R. J.; Wofsky, S. C.; Logan, J. A. *Nature* **1986**, *321*, 759.
(2) Friedl, R. R.; Sander, S. P. *J. Phys. Chem.* **1989**, *93*, 4756.
(3) Anderson, J. G.; Brune, W. H.; Lloyd, S. H.; Toohey, D. W.; Sander, S. P.; Starr, W. L.; Loewenstein, M.; Podolske, J. R. *J. Geophys. Res.* **1989**, *94*, 11480.
(4) Nicovich, J. M.; Kreutter, K. D.; Shackelford, C. J.; Wine, P. H. *Chem. Phys. Lett.* **1991**, *179*, 367.
(5) Vaida, V.; Solomon, S.; Richard, E. C.; Rühl, E.; Jefferson, A. *Nature* **1989**, *342*, 405.
(6) Wahner, A.; Schiller, C. J. *J. Geophys. Res.* **1992**, *97*, 8047.
(7) Sanders, R. W.; Solomon, S.; Smith, J. P.; Perliski, L.; Miller, H. L.; Mount, G. H.; Keys, J. G.; Schmeltekopf, A. L. *J. Geophys. Res.* **1993**, *98*, 7219.
(8) Brandtjen, R.; Klüpfel, T.; Perner, D. *Geophys. Res. Lett.* **1994**, *21*, 1363.
(9) Rühl, E.; Jefferson, A.; Vaida, V. *J. Phys. Chem.* **1990**, *94*, 2990.
(10) Bishenden, E.; Donaldson, D. J. *J. Chem. Phys.* **1993**, *99*, 3129.
(11) Bishenden, E.; Donaldson, D. J. *J. Chem. Phys.* **1994**, *101*, 9565.
(12) Davis, H. F.; Lee, Y. T. *J. Phys. Chem.* **1992**, *96*, 5681.
(13) Davis, H. F.; Lee, Y. T. *J. Chem. Phys.* **1996**, *105*, 8142.
(14) Rockland, U.; Baumgärtel, H.; Rühl, E.; Lösking, O.; Müller, H. S. P.; Willner, H. *Ber. Bunsen-Ges. Phys. Chem.* **1995**, *99*, 969.
(15) Baumert, T.; Herek, J. L.; Zewail, A. H. *J. Chem. Phys.* **1993**, *99*, 4430.
(16) Pursell, C. J.; Conyers, J.; Alapat, P.; Parveen, R. *J. Phys. Chem.* **1995**, *99*, 10433.
(17) Cox, R. A.; Hayman, G. D. *Nature* **1988**, *332*, 796.
(18) Delmdahl, R. F.; Baumgärtel, S.; Gericke, K.-H. *J. Chem. Phys.* **1996**, *104*, 2883.
(19) Furlan, A.; Scheld, H. A.; Huber, J. R. *J. Chem. Phys.* **1997**, *106*, 6538.
(20) Roth, M.; Maul, C.; Gericke, K.-H. *J. Chem. Phys.* **1997**, *107*, 10582.
(21) Bishenden, E.; Haddock, J.; Donaldson, D. J. *J. Phys. Chem.* **1991**, *95*, 2113.
(22) Bishenden, E.; Haddock, J.; Donaldson, D. J. *J. Phys. Chem.* **1992**, *96*, 6513.
(23) Lawrence, W. G.; Clemitshaw, K. C.; Apkarian, V. A. *J. Geophys. Res.* **1990**, *95*, 18591.
(24) Vaida, V.; Simon, J. D. *Science* **1995**, *268*, 1443.
(25) Wahner, A.; Tyndall, G. S.; Ravishankara, A. R. *J. Phys. Chem.* **1987**, *91*, 2734.
(26) Baumgärtel, S.; Gericke, K.-H. *Chem. Phys. Lett.* **1994**, *227*, 461.
(27) Derby, R. I.; Hutchinson, W. S. *Inorg. Synth.* **1953**, *4*, 152.
(28) Reinsch, E. A. Private communication.
(29) Mandelman, M.; Nicholls, R. W. *J. Quant. Spectrosc. Radiat. Transfer* **1977**, *17*, 483.
(30) Arepalli, S.; Presser, N.; Robie, D.; Gordon, R. J. *Chem. Phys. Lett.* **1985**, *118*, 88.
(31) Davis, H. F.; Lee, Y. T. *J. Phys. Chem.* **1996**, *100*, 30.
(32) Peterson, K. A.; Werner, H.-J. *J. Chem. Phys.* **1992**, *96*, 8948.
(33) Peterson, K. A.; Werner, H.-J. *J. Chem. Phys.* **1996**, *96*, 9823.